Improving vegetation spatial distribution mapping in arid and on coastal dune systems using GPR in Tottori Prefecture (Japan)

Christopher Gomez[1,2], Jiaqi Liu[3], Jing Wu[4], Frans Persendt[5], Balazs Bradak[6], Yousefi Saleh[7], Danang Sri Hadmoko[2,*]

[1] Kobe University, Faculty of Oceanology, Laboratory of Sediment Hazards and Disaster Risk, Japan
[2] Universitas Gadjah Mada, Department of Geography, PSBA Laboratory, Yogyakarta, Indonesia
[3] Tottori University, Dry Land Research Centre, Japan
[4] Tsukuba Meteorological Research Institute, Japan
[5] University of Namibia, Namibia
[6] Kobe University, Faculty of Oceanology, Laboratory of Extraterrestrial Oceanography, Japan
[7] Soil Conservation and Watershed Management Research Department, Chaharmahal and Bakhtiari Agricultural and Natural Resources Research and Education Center, Iran
* Corresponding author: hadmoko@ugm.ac.id

ABSTRACT

In this article, desertification and dune progression over vegetation was quantified using remote sensing data. However, vegetation buried under sand blowout could not be counted using this method. Therefore, to estimate the extent of buried vegetation, a GPR campaign was conducted over the coastal sand-dune of Tottori Prefecture (Japan) in combination with a high-resolution topographic UAV-based survey of the topography. The results show that buried vegetation exists underneath sand-blowout, especially near the dune ridges, and can extend from 20 to 30 meters further than the estimate based on airborne remote sensing. Furthermore, the presence of palaeo-vegetation in palaeodune layers also provides the information on the long-term evolution of sand dunes, which can be used to reconstruct Quaternary coastal environments.

1. Introduction

Desertification is one of the challenging results of climate-change and anthropogenic land-degradation (Kasas 1995; Stringer 2008). It threatens biodiversity (Musila et al. 2001), modify climates at the regional scale and can even destabilize food production and economic chains.

The progression of sand against vegetation is particularly acute on coastal sand dune, where urbanization, recreational and touristic activities, erosion from climate change, from anthropogenic origin, or from extreme events (Opelt and Berg 2004; Lee et al. 2006; Lavigne et al. 2009) are all adding supplementary pressure to the bio-geomorphologic system. Despites negative impacts from a human ethics and economic perspective, aeolian sand movement on coastal dunes is a natural process that responds to climate fluctuations, and without human intervention, vegetation is also controlling the erosion from waves runup (Feagin et al. 2019), resulting in complex systems, with complex effects on vegetation. Indeed, the variable geomorphologic units can generate localized micro-climate increasing the species richness and diversity (Ranwell 1972; Kenworthy 1990) and contributing to the diversity generated by nutrients, pH, earthiness and rate of change (Yu and Rhew 2007). Dune mobility is thus displacing vegetation, while creating local diversity.

From a management perspective, however, dune mobility has been proven to negatively impact economic activities (Maun and Baye 1989, Martinez et al. 1997; Levin et al. 2006), so that the local communities and the authorities have attempted to fix the fluctuations of this frontline using vegetation planting (Menashe 1998; Van Loon-Steensma and Schelfhout 2017; UNCDD 2022) and a combination of imported soil and plants (Hong and Lee 2016). This management relies on a knowledge of: (a) the spatial distribution of vegetation, which is assessed by remote sensing (Laporte-Fauret et al. 2020) to extract notably the NDVI index (Levin et al. 2006); and (b) the dynamic processes from flume and field experiments, which have led to the generation of "factor of safety". It expresses the role of the plant in increasing the stability of a sand dune against wave runup for instance (1 and 2 in Laporte-Fauret et al. 2020):

$$\vartheta = -\frac{31.809}{[-31.809 + (0.034 \times a)]} \qquad (1)$$

$$\vartheta = -\frac{48.039}{[-48.039 + (0.027 \times a) + (0.005 \times b) + (8.2 \times c)]} \qquad (2)$$

where a is the above ground biomass, b is the number of leaves per square meter and c is the average stem circumference in cm (cf. Feagin et al. (2019) for further details on the data and calculation). In both empirical equations, the emphasis has been given to the aerial part of the vegetation, but using four (4) different species (Sesuvium portulacastrum, Panicum amarum, Ipomoea pescapre and Spatina patens), however Feagin et al. (2019) have also argued that the part below ground have an impact on wave erosion. Extending this idea, buried vegetation and root systems certainly have an effect on the erodibility of the coastal sand dunes, would it be from the action of waves or wind-blows. Consequently, understanding the distribution of buried vegetation and roots in the subsurface of coastal sand dunes is essential to understand the balance at the frontlines between vegetation and sand surface, and for any accurate estimation of sand-dunes biomass.

For this purpose, one method that has proven to be particularly effective in surveying the subsurface of coastal and other sand dunes is Ground Penetrating Radar (GPR). GPR is an electromagnetic method that relies on the change of velocity and reflected energy from linear and punctual objects in the ground, with change in the dielectric permittivity being the main reason for those variations. By recording series of single radar traces, juxtaposed one to another, it is then possible to obtain an "image" of the subsurface. This technology began to emerge in the 1960s and was well explained by the end of the 20th Century (Davis and Annan 1989; Conyers and Goodman 1997; Reynolds 1997). For coastal dunes, originally, digging deep trenches in unconsolidated sediments was lined with difficulties, and GPR started to reveal the complex internal structure of coastal dunes over long-transects in otherwise inaccessible settings (Neal and Roberts 2001), as well as dunes in other environments – e.g. in Antarctica (Bristow et al. 2010a).

Comparing trenches visuals with GPR data, strong reflectors in sand dunes have been linked to humic horizons (Neal and Roberts 2001; Gomez et al. 2010) and other paleosols buried during dune movement (Buynevich et al. 2007). Similarly, reflectors of lower amplitude and inclined at angles related to the friction angle of dry sand (between 30 and 37 degrees) and typical of the sand dune processes, have also been identified in most of the research on sand dune internal structure (e.g. Kain et al. 2014). This relation between GPR reflectors and sedimentary units has then allowed for large-scale GPR surveys in the Namib Desert (Chandlers et al. 2022), providing then extensive images of the subsurface structure.

In combination with dating from Quartz optically stimulated luminescence, the different layers identified with GPR could then be used to define the age of different paleosurfaces in sand dunes from Soulac to Biarritz in the Southwest France for instance (Bertran et al. 2020), showing that aridification periods also coincided with high-wind speeds during the last 25ka to 14ka. Such methods have also been used and extended to other environments to make inferences on extra-terrestrial bodies (e.g. Bristow et al. 2010b).

It then demonstrates the importance of sand dunes to assess aeolian activity (Anthony et al. 2010), how sea-level changes influenced the coasts (Skornik et al. 2008) as well how sand dunes can be used to asses past-meteorological variations (e.g. Sommerville et al. 2007).

Because sand dunes are mostly made of homogeneous well-sorted grain-sizes (from the GPR perspective), they are well indicated for GPR studies (Braton and Montagu 2004) and the search for buried vegetation and roots. When tree roots have a pluricentimetre diameter, it is even possible to measure the diameter from GPR, as it has been shown from 500 MHz – or higher frequency – antenna tests (Barton and Montaagu 2004). In other words, the relative homogeneity of the sand blowouts makes
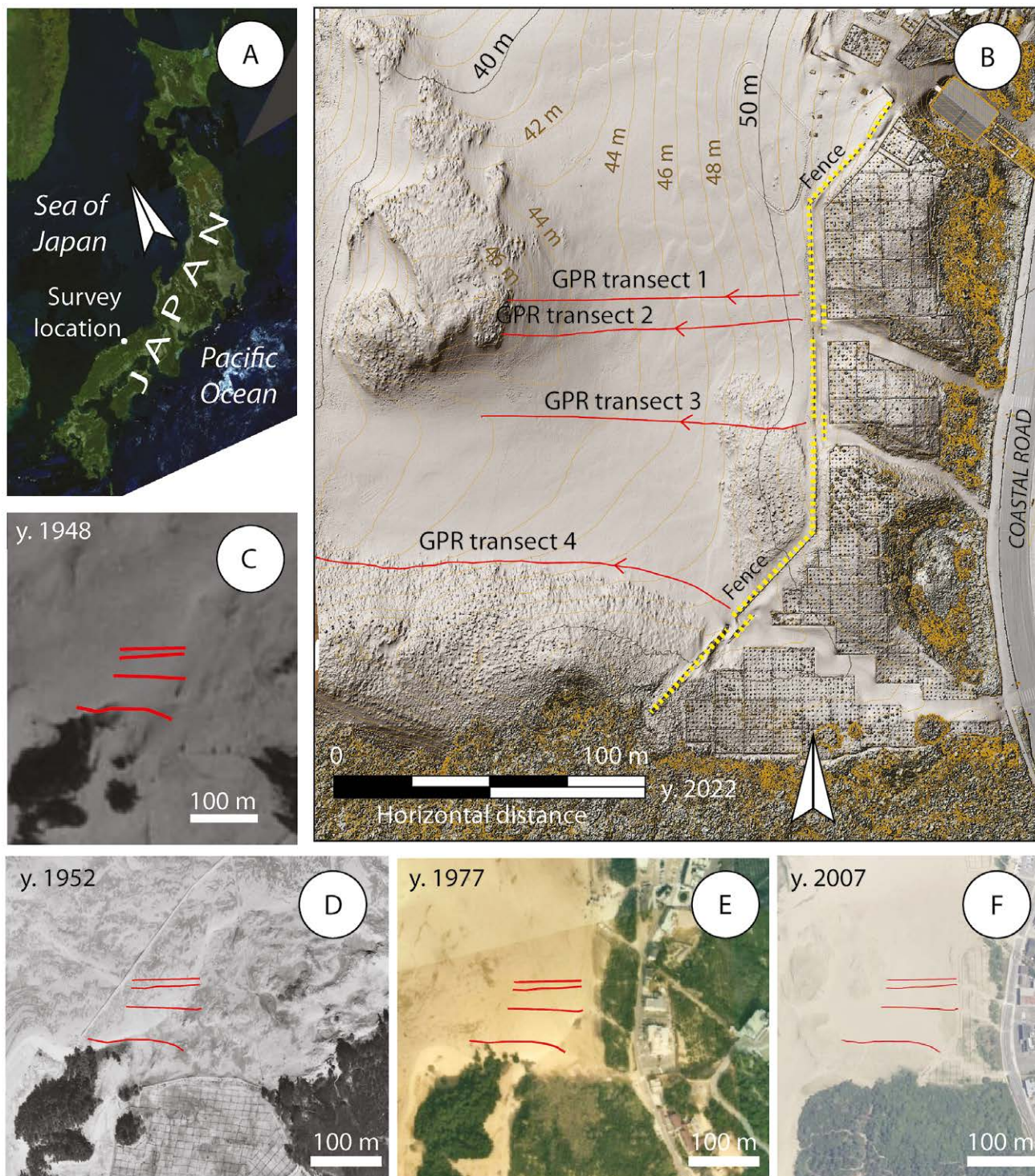
Fig. 1 Study location on (A) the West Coast of Japan, where (B) 4 GPR transects were acquired in an East-West direction. The location during the historical period shows variations in the sand dune land cover, although in (C) 1948, (D) 1952, (E) 1977 and (F) 2007, no major vegetation encroachment is recorded in the area. Only transect 4 has been in vegetated areas (1948 and 1952). The yellow-dotted line marks the fence acting as a sand-barrier.

the identification of punctual objects, such as buried anthropogenic elements and vegetation and roots, easier than in environments that are block-rich and where the material is poorly sorted (e.g. Gomez and Lavigne 2010). And, even in well-sorted environments, the variation in grain-sizes can generate artefact-limits, which can be difficult to identify (Gomez et al. 2008, 2009). Furthermore, to the contrary of sand dunes, moisture-rich silty and clay-rich soils can limit the contrasts between the substratum and the tree roots, leading to further difficulties in interpreting the results (Butnor et al. 2001). Coastal sand dunes are thus an ideal environment to study buried vegetation and roots using GPR, and thus retrieve the presence of otherwise invisible biomass and vegetation.

The present study is thus aiming to image the subsurface in the vicinity of low-grass vegetation in order to assess whether vegetation extends further underneath the sand, remaining invisible to other airborne remote sensing techniques. These techniques are essential, because, by law, one is not authorized to dig a trench or a hole in the Tottori Sand Dune over environmental concerns.

2. Study area

The present research was conducted at the Tottori Sand dune in Tottori Prefecture, Japan (Fig. 1).

The coastal sand dune is located on the West Coast of Japan and fully ex-tend along a 16 km long band, which is about 1 km in width. The sand dune has been dated from tephrochronology to be 50 ka to 70 ka (Naruse 1989), with this sand-dominated feature trapped between the sea and other coastal plain deposits (Murayama et al. 1963; Tamura et al. 2010). Although the Tottori prefecture is not an arid area per se with annual rainfall ranging between 1300 mm/year to 2000 mm/year in the last 20 years (JMA 2023).

In the present survey, we focused on the area named Hamasaka (Tamura et al. 2011), at the landward-edge of the dune, where the dune is active and sand fencing has been installed. Fencing is necessary because the main wind directions oscillate between WNW and NNW at velocities >8 m/s 3.5% of the time, and >12 m/s about 1% of the time (Tamura et al. 2011). Using GPR, Tamura et al. (2010, 2011a, 2011b) have imaged the Tottori sand dune along two parallel transects of 600 m and 1,200 m, which provide an overall overview of the dune structure. But there has been no localized study working on the vegetation, nor has there been detailed imaging of the first 2 m, as previous studies have concentrated on the general structure.

On the sand-dunes of Tottori prefecture, a total of 132 vascular plant species have been found, among which 4 are endemic species, distribution of which is

Total error	Long. error (m)	Lat. error (m)	Alt. error (m)
Control points	0.025	0.025	0.003
Check point	0.025	0.031	0.031

Fig. 2 Topographic data acquisition along a 280 m × 290 m square using the DJI MATRICE 300RTK UAV in combination with Ground Control Points and Check Points recorded by GNSS commercialized by TOPCON.

linked to the dunes' dynamics and the anthropogenic activities (Iwasato and Nagamatsu 2018).

3. Methodology

3.1 Topographic data and orthophotographs

As sand dunes change topography and surface vary rapidly, notably under the influence of wind blowout, the topography and the imagery was acquired within a few hours of the GPR data, to assure that the topography is conform to the GPR transect, and also because high-resolution imagery allows to confirm the length of the transects recorded by the GPR.

The UAV used for the survey is a DJI® Matrice 300 RTK (Fig. 2), which was flown using automatic flight. From the UAV a set of photographs was taken using a Zenmuse P1 camera at an altitude of 30 m, with a flight speed of 3 m/s, and with an overlap ratio of 80% laterally and in the direction of the flight.

In combination with the Ground Control Points recorded using a GNSS (Global Navigation Satellite System) commercialized by TOPCON® (Fig. 2), the photographs were processed in the SfM-MVS (Structure from Motion-Multiple View Stereophotogrammetry) processing software Agisoft® Metashape generating an orthophotograph at a resolution of 0.01 m/pixel (for detailed explanation on the methods, see Gomez 2022), and an altitude error at the check points of 0.031 m, which is below error that would influence the result of the GPR results.

3.2 Ground Penetrating Radar data acquisition and processing

The internal architecture of the sand dune in the survey area was imaged using a Ground Penetrating Radar (GPR) Mala® ProEx mounted with a shielded 800 MHz antenna, from which distance was measured with a coding wheel. Four transects of length 93 m to 178 m were recorded starting landward, and directed towards the sea in an East–West direction (Fig. 1). The accuracy of the GPR signal is related to the vertical resolution (R) of the collected data (3), which has been calculated to be equivalent to the radial resolution, which can be approximated to be 1/4 of the wavelength (Reynolds 1997), and which can be determined as the velocity (V) divided by the nominal frequency of the antenna (f):

$$R = \frac{1}{4}\frac{V}{f} \tag{3}$$

In such a way, the ratio of velocity over frequency for a 800 MHz antenna in free-space (velocity 299,792,458 m/s) is 37.47 cm, and it becomes 18.75 cm (velocity 150,000,000 m/s), so that the maximum accuracy that is attainable with the present dataset is 4.6875 cm. In other words, the 800 MHz antenna

will not be able to image single roots or single stems in vegetation, but it will provide an image when there are "clots" of vegetation and roots and soil, or wetter sand that can create a local reflector.

The collected GPR data were then processed following a 7 steps procedure (standard procedure found for instance in (Ettinger et al. 2014; Gomez et al. 2008, 2009; Gomez and Lavigne 2010): (1) the mean-time zero correction, so that the 0 corresponds to the topographic surface; (2) DEWOW function application to limit the effects of the surface "ringing effect"; (3) Gain correction compensation with AGC Gain correction, with an empirical value of 1.1 dB/m and a maximum amplitude of 10k dB/m to avoid over-saturation; (4) based on the slopes of the hyperbolae, the average velocity was set to 1.5 m/ns (typical of dry unsaturated and dry sands); (5) Migration of the radargram for velocity, using a unit-velocity field and migration for topography based on the topographic data extracted from the topographic data acquired by UAV.

4. Results

The radargram extracted along transect 1 (Fig. 3) is topographically lower seaward. The internal structure of the radargram is composed of sets of 30 to 35 degrees (Fig. 3-B) with two areas of ~30 m leeward (Fig. 3-C), and ~25 m in the upper area, where a < 1 m thick sets of layers are displaying series of units' sub-parallel to the present topography. There is a sharp contact between these sets of units near the surface and the underlying units at a steeper angle. The two units near the surface (a) and (b) (Fig. 3-B), are the latest deposits, and underneath (b) two generations of accumulations separated by 'reactivation zone' (c and d) serve as a base to the most recent accumulations (b). Underneath the inclined layers, there is a buried unit (f) that resembles the b, c, d units.

Both zooms C and D (Fig. 3) are also displaying a high-concentration of hyperbolae (the sets of black and white arrows). The black-arrows are for hyperbolae are generated by objects located at the surface. In the majority of cases, the hyperbolae are aligned in sets of single layers, instead of being mixed at different depths. The hyperbolae have all very close slope angles in both the rising and falling limbs, across the radargram confirming the similarity of the material.

At both the beginning and the end of the transect, the concentration of hyperbolae is linked to the presence of punctual objects, which are related to the dune vegetation, and invisible from the surface.

The second transect, (Fig. 4) is parallel to transect 1 (Fig. 3) and it presents similarities with the later. The roots or buried aerial part of the vegetation creates a large number of hyperbolae between 72 m and the end of the transects. The hyperbolae are again concentrated in one single layer (Fig. 4-B)
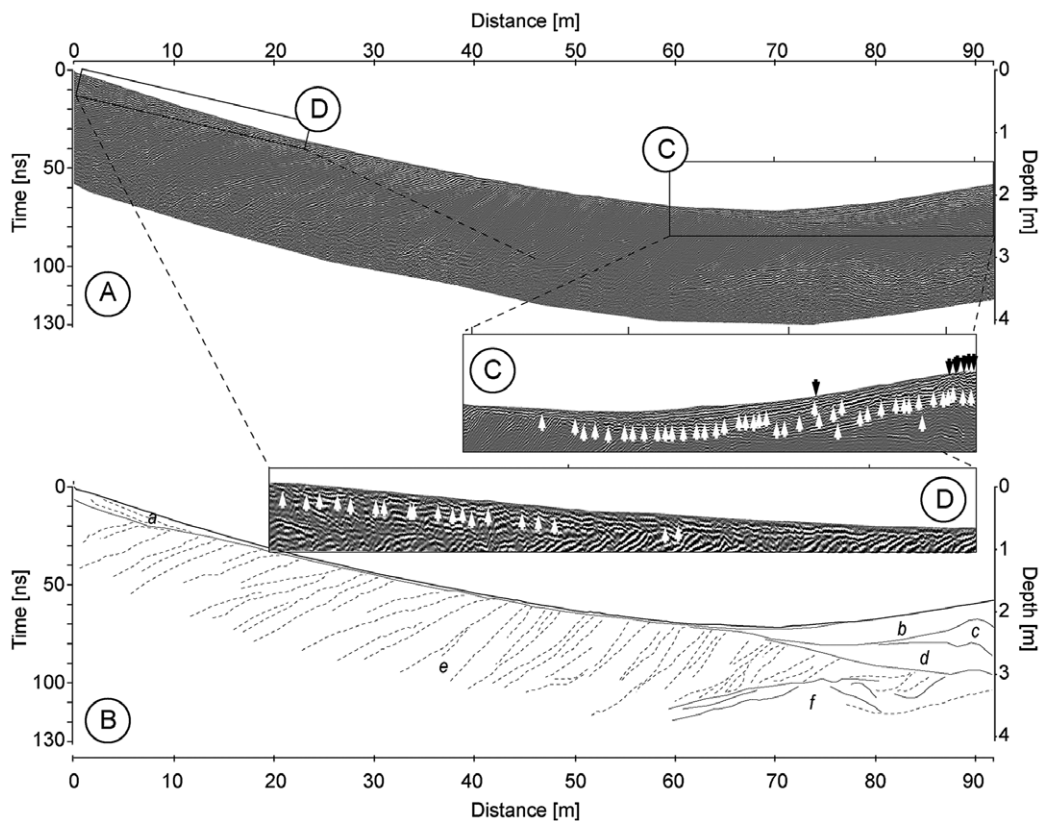
Fig. 3 The radargram acquired at transect 1 and the explanation of both the major units and the distribution of the punctual objects in the subsurface noted as black and white arrows in the zoom; please note that these are not exhaustive lists and other hyperbolae exists, although their interpretation was uncertain (High-resolution files available upon request).
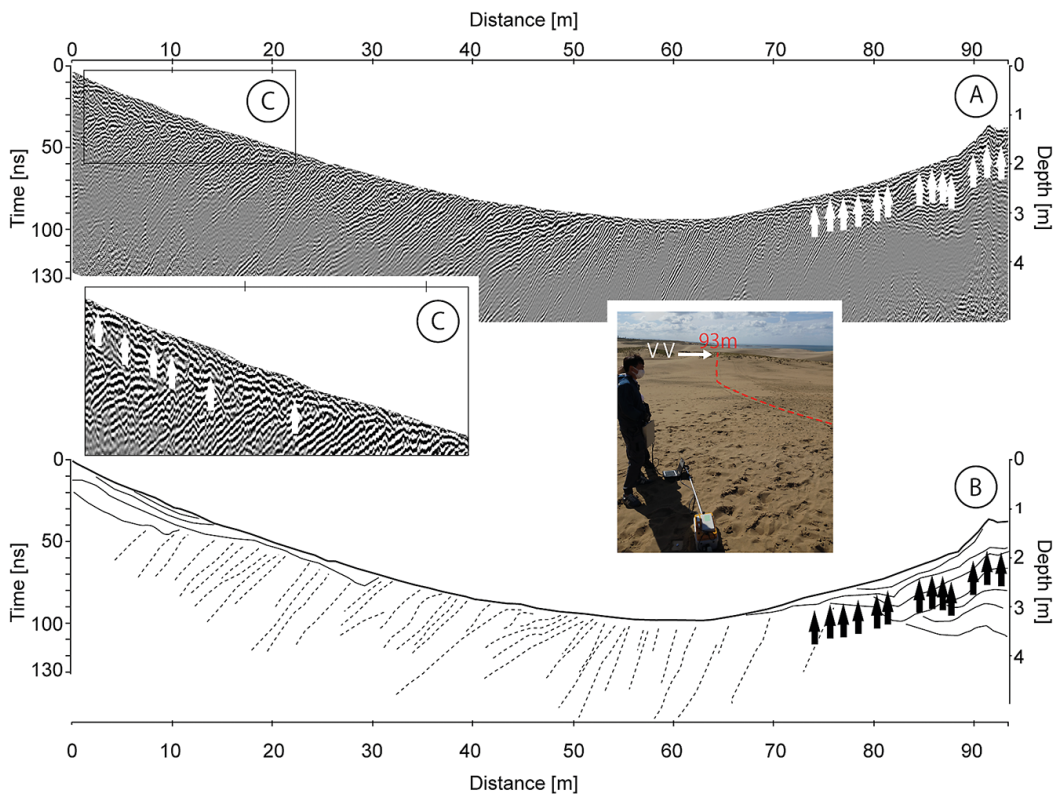
Fig. 4 Transect 2 divided between the radargrams (A), the limits between the different units (B) and a Zoom showing a potential blowout sets of layers (C). A photograph also shows the place where the GPR was dragged (High-resolution files available upon request).
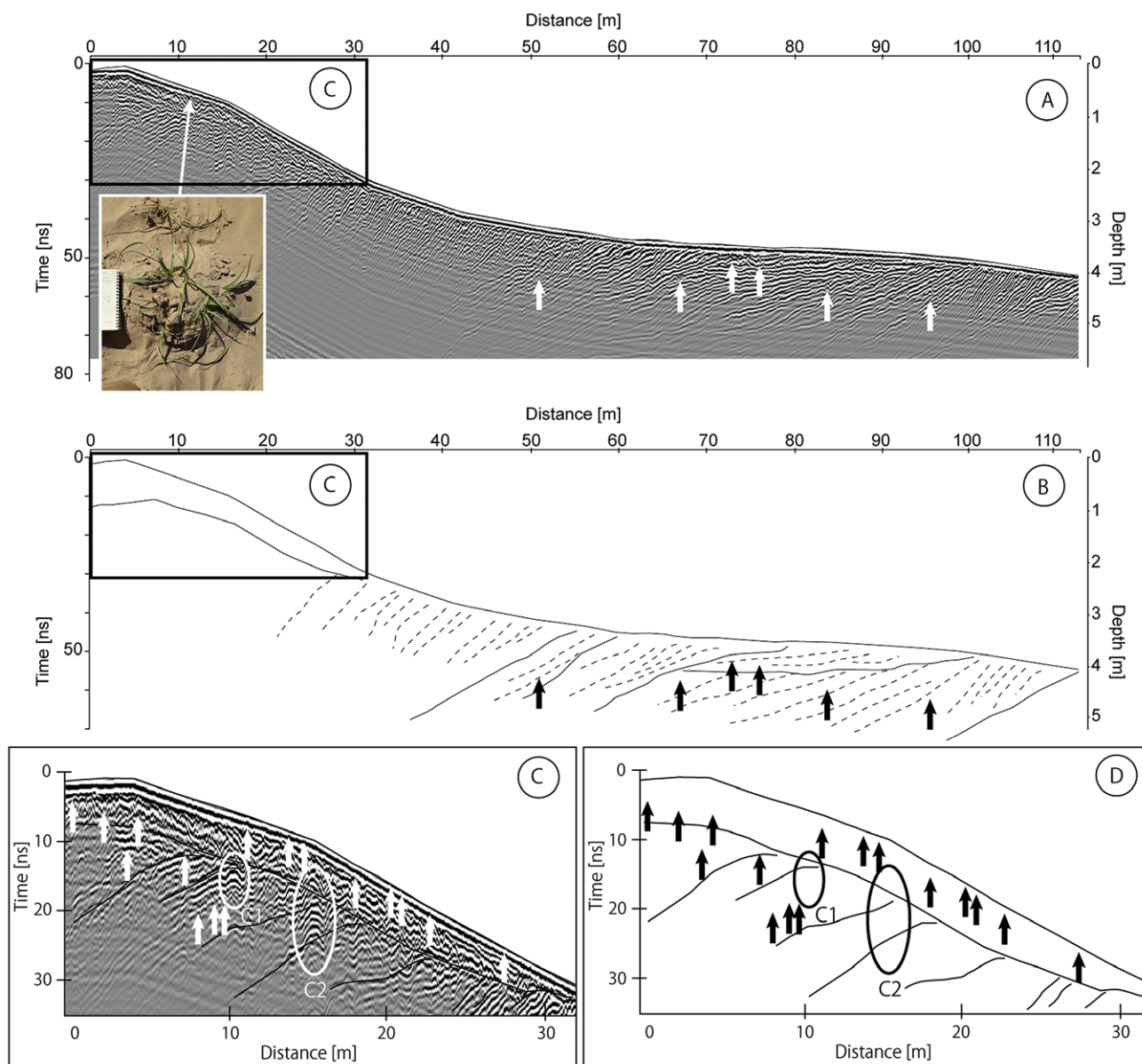
Fig. 5 Transect 3 acquired by GPR (A) and of which the major units have been extracted (B). The first 30 m shows a complex set of layers and hyperbolae (C), where two hyperbolae (C1 and C2) also suggest the presence of foreign material (D) (High-resolution files available upon request).

although vegetation only appears towards the end of the transect near the ridge at 90 m distance (VV on the photograph at the end of the transect on Fig. 4). At the beginning of the transect, there is also, as in transect 1, a series of subhorizontal layers that forms a discontinuity with the slanted layers underneath. With the white arrows, the clearly visible hyperbolae have been identified, although there are others, of which only a small portion is visible (and thus were not marked). At the centre of the transect, between 45 and 50 m, there is one hyperbolae that was not present in transect 1. The signal amplitude at the reflector is stronger than for other hyperbolae and may be due to a foreign object.

The third transect (Fig. 5) is decreasing seaward and not climbing up towards the end as with transects 1 and 2. At this location the first 30 m display a similar

pattern as in transects 1 and 2. A sub-horizontal layer is forming a discontinuity with the underlying layers, but this time the layer a slightly thinner (~80 cm) and it is very rich in hyperbolae (Fig. 5-A and B). The hyperbolae are not confined to this layer, but they are also to be found in the slanted layers underneath. (Fig. 5-C). Hyperbolae that have a tip reaching the surface have been identified to be related to vegetation at the surface (cf. photograph in Fig. 5), and among the hyperbolae, there are two hyperbolae with strong reflectors (C1 and C2), with vertical repeats suggesting that material like iron composes the reflectors showing anthropogenic impacts.

The last recorded transect (Transect 4: Fig. 6) is the longest, with 178 m, and it shows further complexity compared to the other transects. If the subsurface is dominated by sub-parallel units at a slanted angle of

30 to 35 degrees (like the other transects), there is a buried dune crest with a change of dipping angles in the layers (Fig. 6-B and C and Zoom F), as well as on the opposite a set of concave units (Fig. 6-G). On Fig. 6, the entire transects presents hyperbolae in the immediate subsurface (comparing with the previous transect on Fig. 5, one can observe that in transect 4 the first few centimetres are discontinuous in-stead of being dominated by a "uniform" surface and few-first decimetres).

Underneath this layer, there is a set of hyperbolae in the first 30 m, corresponding to the palaeo-crest of a dune, as well as along layers with an apparent dip (not in 3D) towards the sea. These series of hyperbolae have been further identified with red arrows (Fig. 6). These groups of hyperbolae are mostly linked to reflectors of higher amplitudes, rather than the layers defined by sets of low amplitude signal. At the end of the transect (from 140 m) an area that is flatter, topographically, is defined by a group of "plate-like" layers, with reflectors hyperbolae (Fig. 6-G).

5. Discussion

The GPR investigation of a 280 m × 290 m area of the sand dune has shown that the subsurface is dominated in its lower part by a slanted series of layers with an angle be-tween 30 and 37 degrees (one will note that they just seem steeper on the figures due to the scale relation between vertical and horizontal values). These layers reach the surface except at the end on
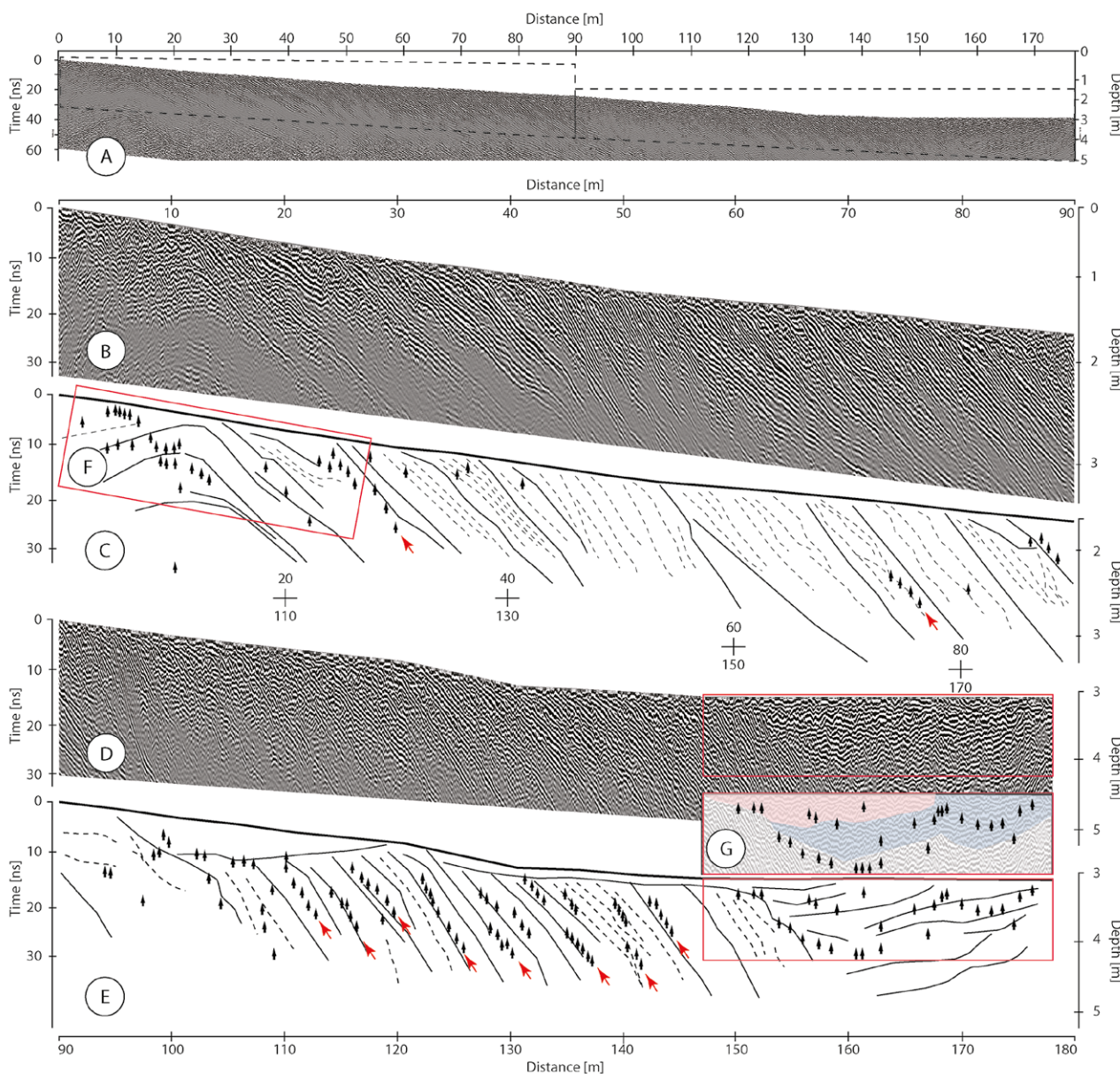
Fig. 6 Transect 4 in its full length (A), and divided between the first 90 m (B and C) and the last 87 m (D and E). The zoom F and G show two opposite layering patterns, with convex and concave shapes. The hyperbolae are shown with black arrows, and the alignments along slanted layers are further demonstrated using red arrows (High-resolution files available upon request).

the topographic highs and the low-topographic (Transect 4). At these locations, other layers are placed over these slanted layers series to form discontinuities. The layering of these top layers is subparallel to the surface, or showing a "plate" shape, as though infilling a topographic hole. As the dune is composed of rather homogeneous sand-grains, punctual objects creating hyperbolae are either due to objects introduced by humans (e.g. in transect 4 the two ringing hyperbolae that could typically be concrete blocks with steel inside), or due to vegetation roots or buried vegetation (at 40–50 m above sea level, it is too high to be driftwood or objects brought by tidal activities). The near-surface hyperbolae and the hyperbolae aligned in layers can thus be confidently attributed to buried vegetation or roots. This interpretation is further consistent with wind blowout locations near ridges or in front of the sand-fences, and for the buried alignments, it shows times of "lower" activity, when the dune is moving more slowly and the vegetation has sufficient time to encroach on the now buried surfaces.

Compared with the existing GPR imaging of the Tottori sand dune (Tamura et al. 2010, 2011a, 2011b), the presence of the slanted layers in units linked to reactivation period is consistent with the finding of the present study, where layers are included in units separated by higher-amplitude data. Furthermore, and although the transects were not taken in the same location as the three transects that are presented in the three papers of Tamura et al. (2010, 2011a, 2011b), most of the units can be attributed to present wind activity, with the layers the most inland corresponding to dates 200 to 300 years old and later. In the lower section of transect 4 however, the buried dune ridge could be linked to the Pleistocene Dune, based on the position proposed by Tamura et al. (2010).

5.1 Sand dune structure

The subsurface units with a slanted angle of 30 to 35 degrees is typical of sand dunes and coastal sand dunes and have been found to form the main
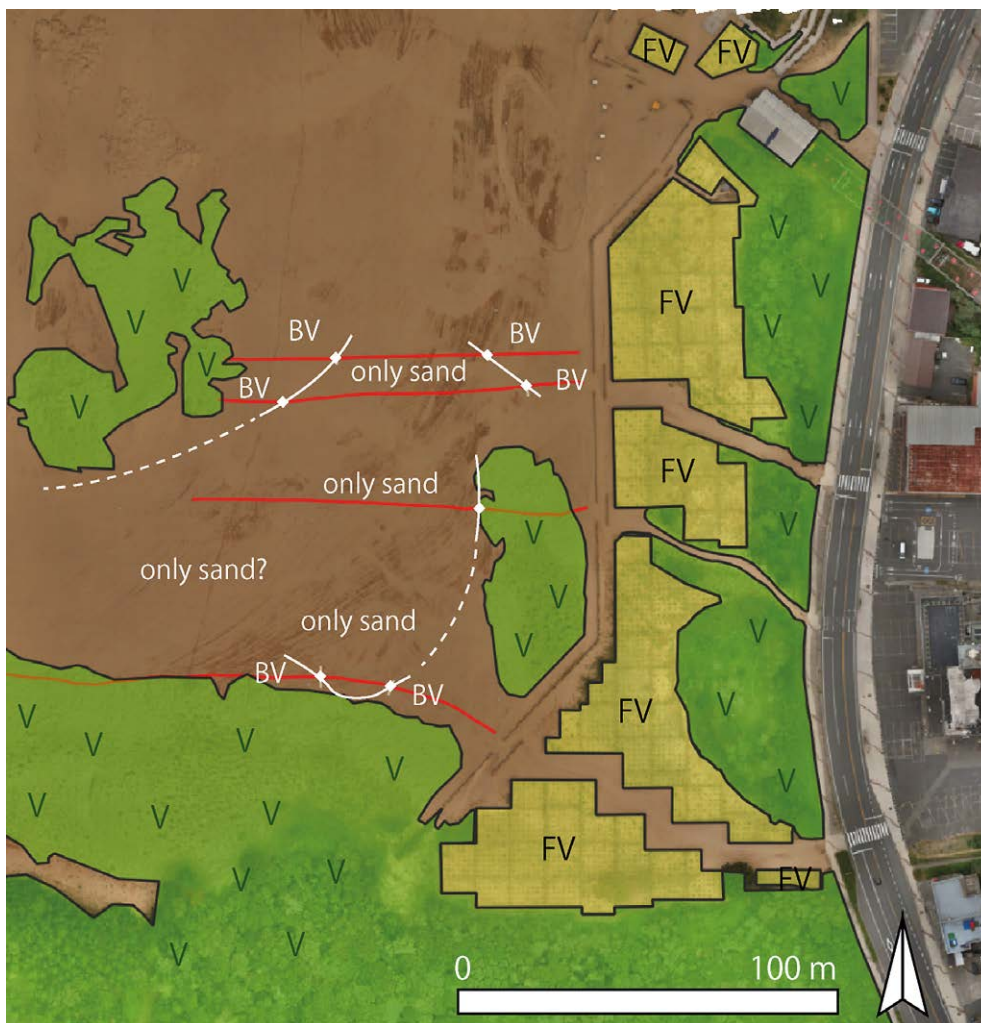
Fig. 7 Distribution of the ground-cover and potential limits of recently buried vegetation (in green with V: vegetation; in yellow with FV: Fenced vegetation; BV: Burried vegetation; the solid white line shows the interpolation of the limit of the near subsurface vegetation; and the dotted line, further interpretation of these limits.

structure of parabolic dunes on the French coast of Acquitaine (Bertran et al. 2020), and also in dunes in other environments, like Antarctica (Bristow et al. 2010b) and the Namib desert (Chandlers et al. 2022). The sand-dunes of the Namib desert, like in Tottori, are also displaying other units towards the top with also truncated units and "superposition surfaces (cf. in Chandlers et al. 2022 Fig. 7 and 8). These types of structures are thus not limited to coastal environment, but typical of wind-deflation and the results of the present study correspond well with the description and interpretation of the radargram from barchane dunes for instance (Fu et al. 2019). These authors have thus related the structure seen on transect 4 in Zoom G to be "trough cross-strata radar facies", with reflections at 28–32 degrees, values that are slightly lower than the 30–35 degrees found in the present study. This discrepancy can be due to the type of sand and its angularity, modifying the repose angle or friction angle of the sand (e.g. Souza Junior et al. 2020), and it can also be associated with the fact that in the present study, we are only examining a system that is inherited and being eroded through with new depositions and movements, meaning that the internal trough cross-strata are not directly related to the present topography.

5.2 Sand dune vegetation and buried vegetation

The interpretation of buried vegetation (whether roots or aerial components of the plant) was found in the upper layers subparallel to the slope, on the stoss side of the dune, which is the location where plants tend to develop first as it is potentially more stable than the steep leeside (facing land in the case of Tottori), as it can be seen from the survey of vegetation establishment in the coastal sand dunes of Israel between 1965 and 1999 (Kutiel et al. 2004). Once the stoss side is more stable, then the lee-side also becomes stable and then vegetation develops.

Buynevich et al. (2017) have used the same GPR and the same antenna in the coastal sand dunes of Lithuania and the Bahamas to image vegetation and roots on dunes. Using the 800 MHz antenna, they have notably imaged windblown buried vegetation as well, proving that the method used in the present survey is replicable, and that this vegetation, once buried indeed generate hyperbolae from punctual objects (e.g. the radargrams of figures 4 and 5 in Buynevich et al. 2017).

5.3 Vegetation estimation and the need for subsurface data

Finally, the findings from GPR show that vegetation and vegetation-roots should ex-tend away from the areas where vegetation is visible at the surface (Fig. 7). Buynevitch et al. (2017) have studied in areas where vegetation is more mature with tree stands and is visible at the surface, but for lower vegetation (grass, etc.) they may disappear fully under blowout and not be counted during remote-sensing assessment of desertification for instance. The results of this study have relevance to hydrological modelling in semi-arid areas as well, especially pertaining to vegetation estimation which plays an important in flood and water resource management in these scarce areas. This is especially true to rainfall-runoff models such as the Namrom and NamPit (Namibia) which rely on vegetation cover estimates of previous year to determine water flux and storage (Hughes and Metzler 1998).

Although the present research is not sufficient to do so, it appears essential to multi-ply GPR assessment of the dune subsurface, in order to better assess the biomass, present on the sand dune. Especially, when vegetation recovered by blowout is not killed in the process, the later could "re-sprawl". Unexpectedly, such research topic has been largely overseen, because data are mostly generated from remote-sensing, and this should become a new research direction.

6. Conclusion

Combining UAV-based SfM-MVS topography and GPR, the now inactive dune sys-tem (most probably Pleistocene) is being eroded and recovered by wind blow-out, which are periodically covered by vegetation. This process seems to have occurred during the palaeodune development, showing periods of stability and periods of "stronger winds". Finally, buried vegetation in the near subsurface can extend 20 to 30 m from an area where vegetation is visible from the surface, and it may be necessary to rethink the limits of vegetation, if one wants to consider more than the mapping of the subaerial organs of plants.

References

Annan, A. P. (2005): Ground penetrating radar in near surface geophysics. In D. K. Butler (Eds): Near-Surface Geophysics. Investigations in Geophysics 13, 357–438, https://doi.org/10.1190/1.9781560801719.ch11.

Anthony, E. J., Mrani-Aloui, M., Hequette, A. (2010): Shoreface sand supply and mid- to late Holocene Aeolian dune formation on the storm-dominated macrotidal coast of the southern North Sea. Marine Geology 276(1–4), 100–104, https://doi.org/10.1016/j.margeo.2010.07.006.

Barton, C. V. M., Montagu, K. D. (20004): Detection of tree roots and determination of root diameters by ground-penetrating radar under optimal conditions. Tree Physiology 24(12), 1323–1331, https://doi.org/10.1093/treephys/24.12.1323.

Bertran, P., Andrieux, E., Bateman, M. D., Fuchs, M., Klinge, M., Marembert, F. (2020): Mapping and chronology of coversands and dunes from the Aquitaine

southwest France. Aeolian Research 47: 100628, https://doi.org/10.1016/j.aeolia.2020.100628.

Bristow, C. S., Jol, H. M., Augustinus, P., Wallis, I. (2010a): Slipfaceless 'whaleback' dunes in a polar desert, Victoria Valley, Antarctica, Insights from ground penetrating radar. Geomorphology 114(3), 361–372, https://doi.org/10.1016/j.geomorph.2009.08.001.

Bristow, C. S., Augustinus, P. C., Wallis, I. C., Jol, H. M., Rhodes, E. J. (2010b): Investigation of the age and migration of reversing dunes in Antarctica using GPR and OSL, with implications for GPR on Mars. Earth and Planetary Sciences Letters 289(1–2), 30–42, https://doi.org/10.1016/j.epsl.2009.10.026.

Butnor, J. R., Doolittle, J. A., Kress, L., Cohen, S., Johnsen, K. H. (2001): Use of ground-penetrating radar to study tree roots in the southeastern United States. Tree Physiology 21(17), 1269–2001, https://doi.org/10.1093/treephys/21.17.1269.

Buynevich, I. V., Bitinas, A., Pupienis, D. (2007): Lithological anomalies in a relict coastal dune: Geophysical and palaeoenvironmental markers. Geophysical Research Letters 34(9): L09707, 1–5, https://doi.org/10.1029/2007GL029767.

Buynevich, I. V., Savarese, M., Allen Curran, H., Bitinas, A., Glumac, B., Pupienis, D., Kopcznski, K., Dobrotin, N., Gnivecki, P., Park Boush, L., Damusyte, A. (2017): Sand incursion into temperate (Lithuania) and tropical (the Bahamas) maritime vegetation: georadar visualization of target-rich Aeolian lithosomes. Estuarine Coastal Shelf Sciences 195, 69–75, https://doi.org/10.1016/j.ecss.2017.02.011.

Chandlers, C. L., Rabedaugh, J., McBride, J. H., Morris, T. H., Narteau, C., Arnold, K., Lorenz, R. D., Barnes, J. W., Hayes, A., Rodriguez, S., Rittenour, T. (2022): Near-surface structure of a large linear dune and an associated crossing dune of the northern Namib sand Sea from Ground Penetrating Radar: Implications for the history of large linear dunes on Earth and Titan. Aeolian Research 57:100813, https://doi.org/10.1016/j.aeolia.2022.100813.

Davis, J. L., Annan, A. P. (1989): Ground-penetrating radar for high-resolution mapping of soil and rock stratigraphy. Geophysical Prospecting 37(5), 531–551, https://doi.org/10.1111/j.1365-2478.1989.tb02221.x.

Conyers, L. B., Goodman, D. (1997): Ground-penetrating radar: an introduction for archaeologists. Walnut, Creek, CA: AltaMira Press.

Ettinger, S., Manville, V., Kruse, S., Paris, R. (2014): GPR-derived architecture of a lahar-generated fan at Cotopaxi volcano, Ecuador. Geomorphology 213, 225–239, https://doi.org/10.1016/j.geomorph.2014.01.013.

Feagin, R. A., Furman, M., Salgado, K., Martinez, M. L., Innocenti, R. A., Eubanks, K., Figlus, J., Huff, T. P., Sigren, J., Silva, R. (2019): The role of beach and sand dune vegetation in mediating wave run up erosion. Estuarine Coast Shelf Sciences 219, 97–106, https://doi.org/10.1016/j.ecss.2019.01.018.

Fu, T., Wu, Y., Tan, L., Li, D., Wen, Y. (2019): Imaging the structure and reconstructing the development of a barchan dune using ground-penetrating radar. Geomorphology 341, 192–202, https://doi.org/10.1016/j.geomorph.2019.05.014.

Gomez, C., Lavigne, F., Lespinasse, N., Hadmoko, D. S., Wassmer, P. (2008): Longitudinal structure of

pyroclastic-flow deposits, re-vealed by GPR survey at Merapi Volcano, Java, Indonesia. Journal of Volcanology Geothermal Research 176(4), 439–447, https://doi.org/10.1016/j.jvolgeores.2008.04.012.

Gomez, C., Lavigne, F., Hadmoko, D.S., Lespinasse, N., Wassmer, P. (2009): Block-and-ash flow deposition: A conceptual model from a GPR survey on pyroclastic-flow deposits at Merapi Volcano, Indonesia. Geomorphology 110(3–4), 118–127, https://doi.org/10.1016/j.geomorph.2009.03.024.

Gomez, C., Lavigne, F. (2010): Transverse architecture of lahar terraces, inferred from radargrams: preliminary results from Semeru Volcano, Indonesia. Earth Surface Processes and Landforms 35(9), 1116–1121, https://doi.org/10.1002/esp.2016.

Gomez, C., Lavigne, F., Lespinasse, N. (2010): L'apport du Radar Geologique pour l'etude des impacts geomorphologiques du tsuna-mi du 26 Decembre 2004, In F. Lavigne, R. Paris (Eds.): Le Tsunami du 26 Decembre 2004. Publications de la Sorbonne, Paris, France. 127–136, https://doi.org/10.4000/books.psorbonne.3804.

Gomez, C. (2022): Point-cloud Technologies for Geomorphologists: from data acquisition to processing, Springer, Heidelberg, Germany, https://doi.org/10.1007/978-3-031-10975-1.

Hong, S. H., Lee, E. Y. (2016): Restoration of eroded coastal sand dunes using plant and soil-conditioner mixture. International Biodeterioration and Biodegradation 113, 161–168, https://doi.org/10.1016/j.ibiod.2016.04.021.

Hughes, D. A., Metzler, M. (1998): Assessment of three monthly rainfall-runoff models for estimating the water resource yield of semiarid catchments in Namibia, Hydrological Sciences Journal 43(2), 283–297, https://doi.org/10.1080/02626669809492122.

JMA (2023) Annual Rainfall at the coast of Tottori. Data from the Japanese Meteorological Agency (in Japanese), https://www.data.jma.go.jp/obd/stats/etrn/view/annually_a.php?prec_no=69&block_no=1519&year=&month=&day=&view=p5 (accessed on 9 December 2023).

Kain, C., Gomez, C., Wassmer, P., Lavigne, F., Hart, D. (2014): Truncated dunes as evidence of the 2004 tsunami in North Sumatra and environmental recovery post-tsunami. New-Zealand Geographer 70(3), 165–178, https://doi.org/10.1111/nzg.12052.

Kassas, M. (1995): Desertification: a general review. Journal of Arid Environment 30(2), 115–128, https://doi.org/10.1016/S0140-1963(05)80063-1.

Kenworthy, J. B. Botanical surveys. (1990): In W. Ritchie; L. Kingham (Eds.): The St Fergus Coastal Environment: The physical and Biological Characteristics. C.E.M.P. Aberdeen University Research and Industrial Services, Aberdeen, United Kingdom.

Kutiel, P., Cohen, O., Shoshany, M., Shub, M. (2004): Vegetation establishment on the southern Israeli coastal sand dunes between the years 1965 and 1999. Landscape and Urban Planning 67(1–4), 141–156, https://doi.org/10.1016/S0169-2046(03)00035-5.

Laporte-Fauret, Q., Lubac, B., Castelle, B., Michalet, R., Marieu, V., Bombrun, L., Launeau, P., Giraud, M., Normandin, C., Rosebery, D. (2020): Classification of Atlantic Coastal Sand Dune Vegetation Using In Situ,

UAV, and Airborne Hyperspectral Data. Remote Sensing 12(14): 2222, https://doi.org/10.3390/rs12142222.

Lavigne, F., Paris, R., Grancher, D., Wassmer, P., Brunstein, D., Vautier, F., Leone, F., Flohic, F., De Coster, B., Gunawan, T., Gomez, C., Setiawan, A., Cahyadi, R., Fachrizal. (2009): Reconstruction of Tsunami Inland Propagation on December 26, 2004 in Banda Aceh, Indonesia, through Field Investigations. Pure and Applied Geophysics 166, 259–281, https://doi.org/10.1007/s00024-008-0431-8.

Lee, M. S., Do, J. O., Park, M. S., Jung, S., Lee, K. H., Bae, K. S., Park, S. J., Kim, S. B. (2006): Dominance of Lysobacter sp. In the rhizo-sphere of two coastal sand dune plant species, Calystegia soldanella and Elymus mollis. Antonie Van Leuwenhoek International Journal 90, 19–70, https://doi.org/10.1007/s10482-006-9056-z.

Levin, N., Kidron, G. J., Ben-Dor, E. (2006): The spatial and temporal variability of sand erosion across a stabilizing coastal dune field. Sedimentology 53, 697–715, https://doi.org/10.1111/j.1365-3091.2006.00787.x.

Martinez, M. L., Moreno-Casasola, P., Vazquez, G. (1997): Effects of disturbance by sand movement and inundation by water on tropical dune vegetation dynamics. Canadian Journal of Botany 75(11), 2005–2014, https://doi.org/10.1139/b97-912.

Maun, M. A., Baye, P. R. (1989): The ecology of Ammophila breviligulata Fern on coastal dune ecosystem. CRC Critical Review of Aquatic Sciences 1, 661–681.

Menashe, E. (1998): Vegetation and Erosion: A Literature Review. Greenbelt Consulting. 10p. Retrieved from http://www.greenbeltconsulting.com/assets/pdfs/VegetationAndErosion.pdf (accessed on 27 November 2022).

Murayama, M., Isshiki, N., Sakamoto, T. (1963): Tottori hokubu, Tottori nanbu 1:50,000 Geological map. Chishitsu, 1–8 (in Japanese with English abstract).

Musila, W. M., Kinyamario, J. L., Jungerius, P. D. (2001): Vegetation dynamics of coastal sand dunes near Malindi, Kenya. Afrrican Journal of Ecology 39(2), 170–177, https://doi.org/10.1046/j.1365-2028.2001.00294.x.

Iwasato, M., Nagamatsu, D. (2018): Plant species diversity and habitat conditions in a protected large coastal dune area of Western Japan. Landscape and Ecological Engineering 14, 99–113, https://doi.org/10.1007/s11355-017-0334-x.

Naruse, T. (1989): Coastal Sand Dunes in Japan. Geographical Review of Japan 62A, 129–144 (in Japanese), https://doi.org/10.4157/grj1984a.62.2_129.

Neal, A., Roberts, C.L. (2001): Internal structure of a through blowout, determined from migrated ground-penetrating radar profiles. Sedimentology 48(4), 791–810, https://doi.org/10.1046/j.1365-3091.2001.00382.x.

Opelt, L., Berg, G. (2004): Diversity and antagonistic potential of bacteria associated with bryophytes from nutrient poor habitats of Baltic Sea coast. Applied Environmental Microbiology 70(11), 6569–6579, https://doi.org/10.1128/AEM.70.11.6569-6579.2004.

Ranwell, D. S. (1972): Ecology of Salt Marshes and Sand Dunes. Chapman & Hall, London, United Kingdom.

Reynolds, J. M. (1997): An introduction to Applied and Environmental Geophysics. Wiley, Chichester, United Kingdom.

Skornik, K., Gehrels, W. R., Murray, A. S. (2008): Aeolian sand movement and relative sea-level rise in Ho Bugt, western Denmark, during the 'Little Ice Age'. The Holocene 18(6), 951–965, https://doi.org/10.1177/0959683608091800.

Sommerville, A. A., Hansom, J. D., Housley, R. A., Sanderson, D. C. W. (2007): Optically stimulated luminescence (OSL) dating of coastal Aeolian sand accumulation in Sanday, Orkney Islands, Scotland. Holocene 17(5), 627–237, https://doi.org/10.1177/095968360707898.

Souza Junior, P. L., Santos, Junior, O. F., Fontoura, T. B., Freitas Neto, O. (2020): Drained and undrained behavior of an Aeolian sand from Natal, Brazil. Soil Rocks Technical Note 43(2), 1–8, https://doi.org/10.28927/SR.432263.

Stringer, L. C. (2008): Reviewing the International Year of Deserts and Desertification 2006: What contribution towards combating global desertification and implementing the United Nations Convention to Combat Desertification? Journal of Arid Environment 72(11), 2065–2074, https://doi.org/10.1016/j.jaridenv.2008.06.010.

Tamura, T., Kodama, Y., Saitoh, Y., Watanabe, K., Yamaguchi, N., Matsumoto, D. (2010): Ground-penetrating radar profile of the Tottori coastal dunes. Quaternary Research of Japan 49–6, 357–367 (in Japanese), https://doi.org/10.4116/jaqua.49.357.

Tamura, T., Bateman, M. D., Kodama, Y., Saitoh, Y., Watanabe, K., Yamaguchi., Matsumoto, D. (2011a): Building of shore-oblique transverse dune ridges revealed by ground-penetrating radar and optical dating over the last 500 years on Tottori coast, Japan Sea. Geomorphology 132(3–4), 153–166, https://doi.org/10.1016/j.geomorph.2011.05.005.

Tamura, T., Kodama, Y., Bateman, M.D., Saitoh, Y., Watanabe K., Matsumoto, D., Yamaguchi, N. (2011b): Coastal barrier dune con-struction during sea-level highstands in MIS 3 and 5a on Tottori coast-line, Japan. Palaeogeography Palaeoclimatology Palaeocology 308(1–2), 492–501, https://doi.org/10.1016/j.palaeo.2011.05.054.

UNCCD (United Nations Convention to Combat Desertification). (2022): Great Green Wall Initiative. UNCCD, Bonn, Germany, https://www.unccd.int/our-work/ggwi (accessed on 27 November 2022).

Van Loon-Steensma, J. M., Schelfhout, H. A. (2017): Wide green dikes: a sustainable option with benefits for both nature and land-scape values. Land Use Policy 63, 528–538, https://doi.org/10.1016/j.landusepol.2017.02.002.

Yu, K. B., Rhew, H. (2007): Coastal Dunes on the West Coast of Korea; a Geomorphological Perspective. Seoul National University Press, Seoul, Korea.